
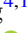








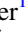





Kepler-730: A Hot Jupiter System with a Close-in, Transiting, Earth-sized Planet

Caleb I. Cañas^{1,2,3,13} , Songhu Wang^{4,14} , Suvrath Mahadevan^{1,2,3} , Chad F. Bender⁵ ,
 Nathan De Lee^{6,7} , Scott W. Fleming⁸ , D. A. García-Hernández^{9,10} , Fred R. Hearty¹ ,
 Steven R. Majewski¹¹ , Alexandre Roman-Lopes¹² , Donald P. Schneider^{1,2} , and Keivan G. Stassun⁷ 

¹ Department of Astronomy & Astrophysics, The Pennsylvania State University, 525 Davey Lab, University Park, PA 16802, USA; canas@psu.edu

² Center for Exoplanets & Habitable Worlds, University Park, PA 16802, USA

³ Penn State Astrobiology Research Center, University Park, PA 16802, USA

⁴ Department of Astronomy, Yale University, New Haven, CT 06511, USA

⁵ Department of Astronomy and Steward Observatory, University of Arizona, Tucson, AZ 85721, USA

⁶ Department of Physics, Geology, and Engineering Technology, Northern Kentucky University, Highland Heights, KY 41099, USA

⁷ Department of Physics & Astronomy, Vanderbilt University, Nashville, TN 37235, USA

⁸ Space Telescope Science Institute, 3700 San Martin Drive, Baltimore, MD 21218, USA

⁹ Instituto de Astrofísica de Canarias (IAC), E-38205 La Laguna, Tenerife, Spain

¹⁰ Universidad de La Laguna (ULL), Departamento de Astrofísica, E-38206 La Laguna, Tenerife, Spain

¹¹ Department of Astronomy, University of Virginia, Charlottesville, VA 22904, USA

¹² Departamento de Física, Facultad de Ciencias, Universidad de La Serena, Cisternas 1200, La Serena, Chile

Received 2018 November 28; revised 2018 December 19; accepted 2018 December 19; published 2019 January 10

Abstract

Kepler-730 is a planetary system hosting a statistically validated hot Jupiter in a 6.49 day orbit and an additional transiting candidate in a 2.85 day orbit. We use spectroscopic radial velocities from the APOGEE-2N instrument, Robo-AO contrast curves, and *Gaia* distance estimates to statistically validate the planetary nature of the additional Earth-sized candidate. We perform astrophysical false positive probability calculations for the candidate using the available *Kepler* data and bolster the statistical validation using radial velocity data to exclude a family of possible binary star solutions. Using a radius estimate for the primary star derived from stellar models, we compute radii of $1.100^{+0.047}_{-0.050} R_{\text{Jup}}$ and $0.140 \pm 0.012 R_{\text{Jup}}$ ($1.57 \pm 0.13 R_{\oplus}$) for Kepler-730b and Kepler-730c, respectively. Kepler-730 is only the second compact system hosting a hot Jupiter with an inner, transiting planet.

Key words: methods: statistical – planetary systems – techniques: photometric – techniques: spectroscopic

1. Introduction

The formation pathways of hot Jupiter planets remains an active area of research (see Dawson & Johnson 2018 and references therein). Current theoretical paradigms for producing these behemoths fall largely into the following two main categories.

- (1) Dynamical migration (e.g., planet–planet scattering, Rasio & Ford 1996; Lidov–Kozai cycling with tidal friction, Wu & Murray 2003; and secular interactions, Wu & Lithwick 2011; Petrovich 2015) violently delivers giant planets to their current orbits, and leaves them dynamically hotter and isolated.
- (2) Hot Jupiters might alternatively be formed via quiescent disk migration (Lin et al. 1996) or in situ formation (Batygin et al. 2016), processes that leave the system dynamically cooler and compact.

Although the presence or absence of additional low-mass planets in close orbital proximity to hot Jupiters provides a zeroth-order test of distinct and competing formation mechanisms, the true occurrence rate for close-in planetary companions to systems with a hot Jupiter remains unclear (Millholland et al. 2017; Wang et al. 2018b).

The radial velocity (RV) precision required for detecting companions with masses comparable to super-Earths, believed to be the most common type of planets in our

Galaxy, are generally at or below $1\text{--}2 \text{ m s}^{-1}$, a detection threshold achieved with the most precise spectrographs (Fischer et al. 2016). Transits by these planets cause drops in stellar brightness smaller than $\sim 0.1\%$, which remain beyond the capabilities of the current generation of wide-field ground-based transit surveys (see Pepper et al. 2018 and references therein).

Hidden planets have started to emerge as higher photometric precision observations of existing planetary systems are obtained. WASP-47b is a typical hot Jupiter that was originally detected with SuperWASP (Hellier et al. 2012). Two additional transiting short-period super-Earths in the system were not detected until subsequent observations were obtained from the *Kepler* spacecraft (Borucki et al. 2010) during the *K2* mission (Becker et al. 2015). Until recently, WASP-47 was the only confirmed hot Jupiter system known with additional close-in planet companions.

Thompson et al. (2018) used all four years of the *Kepler* data to reveal another potential WASP-47-like system, Kepler-730, with a previously known hot Jupiter and an additional transiting planet candidate (also noted by Zhu et al. 2018). This object appears to be an Earth-sized inner planet with an orbital period of 2.85 days, and was not detected in previous searches (Steffen et al. 2012; Huang et al. 2016).

In this Letter, we statistically validate the planetary nature of Kepler-730c based on Doppler velocimetry from the Sloan Digital Sky Survey (SDSS)/APOGEE-2 spectra, Robo-AO high-contrast imaging, and *Kepler* photometry.

¹³ NASA Earth and Space Science Fellow.

¹⁴ *51 Pegasi b* Fellow.

Table 1
APOGEE-2 Observations

BJD _{TDB} ^a	RV ^b (km s ⁻¹)	1σ (km s ⁻¹)	S/N ^c (pixel ⁻¹)
2457879.872229	-68.96	0.28	15
2457908.783554	-69.51	0.48	10
2457918.770521	-69.28	0.28	13
2457919.788244	-69.89	0.43	10
2457920.797865	-69.06	0.23	18
2457938.765117	-69.09	0.46	8
2457940.716527	-68.95	0.48	9
2457941.715177	-69.18	0.31	14
2458007.742691	-69.06	0.46	10
2458188.013655	-68.81	0.44	8
2458209.986371	-69.76	0.92	6
2458234.981317	-68.40	0.63	9
2458237.922857	-68.37	0.56	12
2458238.917524	-67.82	0.53	12
2458261.832167	-68.33	0.42	9
2458290.776784	-69.01	0.29	14

Notes.

^a BJD_{TDB} is the Barycentric Julian Date in the Barycentric Dynamical Time standard.

^b The systemic velocity is $\gamma = -68.94$ km s⁻¹.

^c APOGEE-2N has approximately two pixels per resolution element.

2. Observations and Data Reduction

2.1. APOGEE-2 Radial Velocities

Kepler-730 (KOI-929, KIC 9141746, 2MASS J19021315+4534438, $K_p = 15.65$, $H = 14.18$) was observed from the Apache Point Observatory (APO) between 2017 May 6 and 2018 June 21 as part of the APO Galaxy Evolution Experiment (APOGEE) program (Majewski et al. 2017; Zasowski et al. 2017) to spectroscopically monitor a substantial fraction of the *Kepler* objects of interest (KOIs; Fleming et al. 2015) as part of the SDSS-IV survey (Blanton et al. 2017). We obtained 16 spectra using the high-resolution ($R \sim 22,500$), near-infrared (1.514–1.696 μm), multi-object APOGEE-2N spectrograph (Wilson et al. 2012, 2018, submitted to PASP), mounted on the Sloan 2.5 m telescope (Gunn et al. 2006).

For each observation, the APOGEE-2 data pipeline (Nidever et al. 2015) performs sky subtraction, telluric and barycentric correction, and wavelength and flux calibration. We derived RVs using the maximum-likelihood cross-correlation method presented by Zucker (2003). We identified the best fitting synthetic spectrum in the H -band from a grid of BT-Settl synthetic spectra (Allard et al. 2012) by cross-correlating the APOGEE spectrum with the highest signal-to-noise (S/N) against a grid spanning surface effective temperature ($5300 \leq T_e \leq 5900$, in intervals of 100 K), surface gravity ($3.5 \leq \log g \leq 4.5$, in intervals of 0.5 dex), metallicity ($-0.5 \leq [M/H] \leq 0.5$, in intervals of 0.5 dex), and rotational broadening ($2 \leq v \sin i \leq 50$ km s⁻¹, in intervals of 2 km s⁻¹). The synthetic spectrum with the largest correlation was then used for the final cross-correlation to derive the reported RVs and 1σ uncertainties. These values are listed in Table 1.

2.2. Kepler Photometry

Kepler-730 was observed by *Kepler* for a total of 15 quarters and has 2 planetary candidates, KOI-929.01 and KOI-929.02, with periods of ~ 6.49 days and ~ 2.85 days, respectively.

KOI-929.01 (Kepler-730b) was statistically validated as an exoplanet by Morton et al. (2016) with a false positive probability (FPP) for the signal of $\lesssim 1 \times 10^{-4}$. Prior to the final *Kepler* data release (DR25; Thompson et al. 2018), KOI-929.02 was not considered a planetary candidate.

For the purposes of statistical validation, we analyzed both the *Kepler* simple aperture photometry (SAP) and pre-search data conditioned (PDCSAP) time-series light curves (Stumpe et al. 2012) available at the Mikulski Archive for Space Telescopes (MAST). We detrended light curves using three methods: Cosine Filtering with Autocorrelation Minimization (CoFiAM; Kipping et al. 2013), a polynomial analog of CoFiAM, and a Gaussian process.

CoFiAM regresses the *Kepler* time series using a harmonic (or polynomial) series in a least-squares approach where the optimal detrending function is defined as the one that minimizes the autocorrelation of the residuals. For all of the detrending methods, the portion of the light curve within a factor of 0.6 of the transit duration ($\pm 0.6T_{14}$) from each transit midpoint was excised prior to regression. For the polynomial and CoFiAM methods, each transit was processed separately using the data flanking half a period from each transit midpoint. A 3σ clip on a 20-point rolling median was applied to the detrended light curve to remove any outliers.

We used the *celerite* package to perform the Gaussian process detrending, and assumed a quasi-periodic covariance function, following the procedure in Foreman-Mackey et al. (2017). Each quarter of data was detrended separately and no additional processing was done to the light curve.

To prepare for statistical validation, the transits of the other planetary candidate were removed. The light curve was then phased to the period and time of conjunction listed in DR25 and trimmed to keep data within a phase of three of the transit duration ($\pm 3T_{14}$). KOI-929.01 was detrended solely using a Gaussian process. KOI-929.02 was detrended using the three methods described above (CoFiAM, a polynomial basis, and a Gaussian process). The light curve for the joint fit presented in Section 4 retained all of the data (including any overlapping transits) and each quarter was detrended using a Gaussian process.

3. Planet Validation

3.1. Sky-projected Stellar Companions

For the period range of these planetary candidates, the reliability of the *Kepler* pipeline is $>98\%$ (Thompson et al. 2018). There is also no other target in the *Kepler* threshold crossing events that shares the same period as KOI-929.02, which suggests that the signal for this planetary candidate is unlikely to be produced by instrumental or stellar noise. The *Kepler* photometry in MAST uses a 5×5 pixel mask (see the upper row of Figure 1) to derive the light curves for this system, and each *Kepler* pixel corresponds to $\sim 3''.98$. To investigate any potential background stars in the region, we used the latest data release from *Gaia* (Gaia Collaboration et al. 2018) by searching a $30''$ region around Kepler-730. A total of six stars reside within this region with the closest star, KIC 9141752 ($K_p = 19.1$), located at a sky-projected distance of $6''.57$. No other stars were located within the *Kepler* pixel mask. In the upper right panel of Figure 1, the pixels that were considered source pixels varied by quarter, but rarely flanked

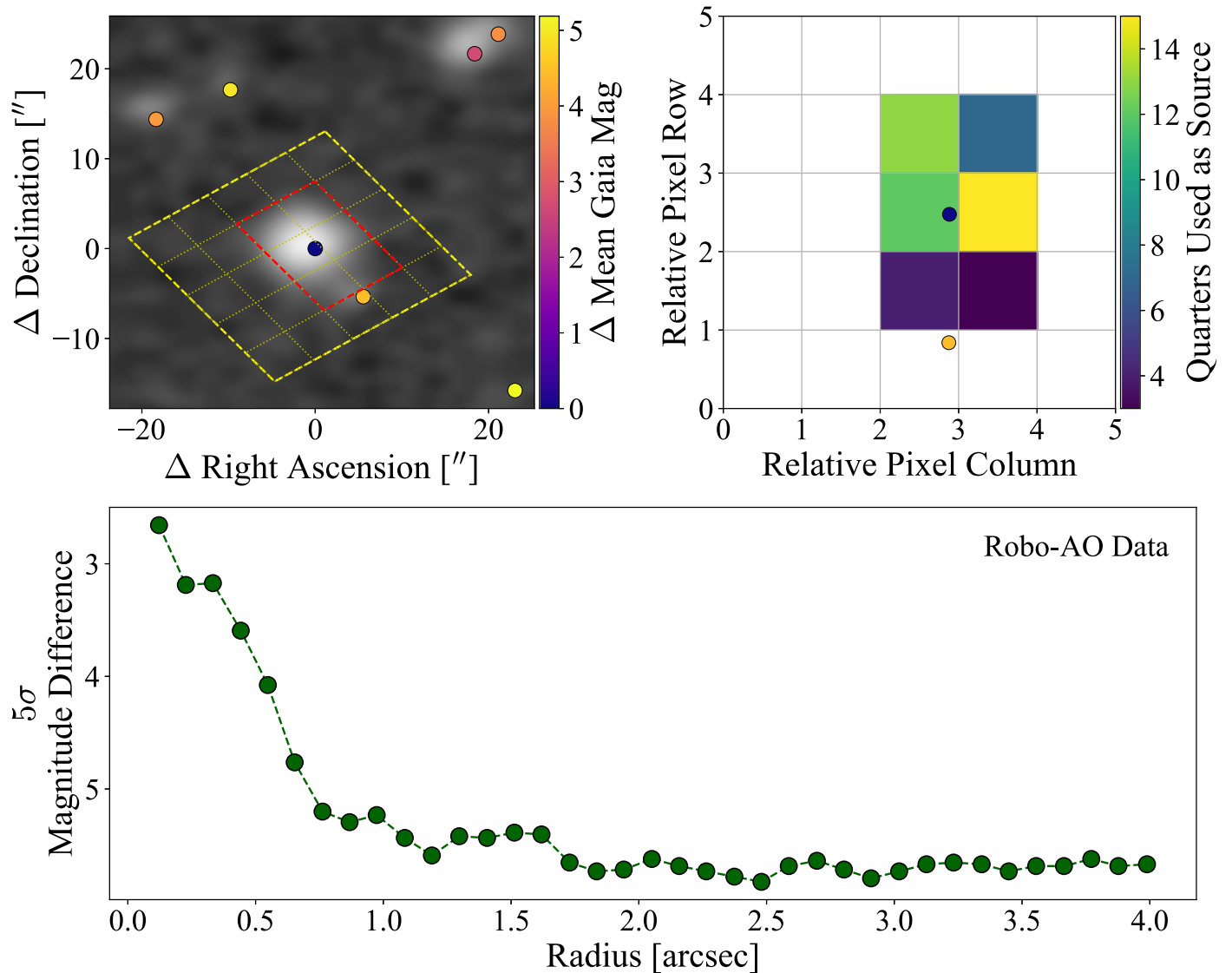


Figure 1. Stellar background around Kepler-730. The upper left panel shows the six stars identified by *Gaia* within a sky-projected distance of $30''$ atop an image of the same region from the Second Palomar Observatory Sky Survey (POSS-II/Red). The closest star, KIC 9141752, has a sky-projected distance of $6''.57$. *Gaia* detected no other stars within the 5×5 pixel mask (yellow grid) used by *Kepler*. The *Kepler* aperture mask (red grid) is highlighted in the upper right panel, with each pixel colored to the number of quarters it used as a source pixel. Only Kepler-730 is contained in the aperture mask where the majority of the flux originates. The bottom panel shows the contrast curve provided by the Robo-AO survey illustrating the threshold magnitude difference to detect a stellar companion as a function of distance from Kepler-730. Robo-AO did not detect any other sources within $4''$ of Kepler-730.

the background star KIC 9141752. Even in the quarters with the smallest aperture mask, the transit of KOI-929.02 persisted.

The Robo-AO adaptive optics survey of the *Kepler* field (Ziegler et al. 2017) has observations of Kepler-730. The survey acquires images in an LP600 filter that serves to approximate the *Kepler* passband at redder wavelengths and mitigate the effects of blue wavelengths on instrumental performance. Robo-AO generates a contrast curve (bottom panel in Figure 1), providing the detection limit as a function of distance from Kepler-730; there are no detected companions within $4''$. Ziegler et al. (2018) demonstrated that the recoverability of asterisms detected by Robo-AO in *Gaia* is $\geq 97\%$ for differences larger than three magnitudes at distances greater than $2''$. While *Gaia* is often unable to resolve asterisms within $\lesssim 1''$ of a star, *Gaia* is more complete than Robo-AO for objects with mean *Gaia* magnitudes of $G > 20$. Together, the *Gaia* and Robo-AO data show that Kepler-730 has no close stellar companions within the *Kepler* aperture mask. Figure 1

displays the stars identified by *Gaia* within $30''$, along with the *Kepler* pixel mask and Robo-AO data.

3.2. False Positive Analysis

We adopted the *vespa* package from Morton et al. (2016) to perform a false positive analysis of Kepler-730b. The algorithm validates a planet statistically by simulating and determining the likelihood of a range of astrophysical false positive scenarios that could generate the observed light curve. *vespa* treats each planetary candidate as the only planet around the host star; this is a conservative view for Kepler-730 given the high reliability of *Kepler* multiplanet systems (e.g., Lissauer et al. 2014). The code generates a population (20,000 systems) for each false positive scenario, including background eclipsing binaries (BEBs), eclipsing binaries (EBs), and hierarchical eclipsing binaries (HEBs), to calculate the likelihoods. We included the two artificial likelihood models from

Table 2
False Positive Probability Analysis of Kepler-730

KOI	FPP	Source	Polynomial	CoFiAM	Gaussian Process
929.02	All	SAP	$(9.1 \pm 2.4) \times 10^{-5}$	$(1.9 \pm 0.33) \times 10^{-4}$	$(8.1 \pm 2.5) \times 10^{-5}$
...	Only EBs/HEBs	SAP	$(2.8 \pm 1.1) \times 10^{-6}$	$(2.6 \pm 0.64) \times 10^{-7}$	$(1.3 \pm 0.19) \times 10^{-7}$
929.01	All	PDCSAP	$(1.7 \pm 1.4) \times 10^{-4}$
...	Only EBs/HEBs	PDCSAP	$(1.7 \pm 1.4) \times 10^{-4}$
929.02	All	PDCSAP	$(1.2 \pm 0.39) \times 10^{-4}$	$(1.2 \pm 0.34) \times 10^{-4}$	$(5.6 \pm 3.2) \times 10^{-5}$
...	Only EBs/HEBs	PDCSAP	$(6.4 \pm 0.99) \times 10^{-8}$	$(5.7 \pm 1.3) \times 10^{-8}$	$(1.4 \pm 0.44) \times 10^{-9}$

Morton et al. (2016) to flag if the transit signal did not fit any astrophysical model. The stellar properties for statistical validation were derived using the `isochrones` package (Morton 2015) setting priors on the (i) 2MASS *JHK* magnitudes (Skrutskie et al. 2006) and *Kepler* magnitudes, (ii) the *Gaia* parallax, (iii) the host star surface gravity, temperature and metallicity from the APOGEE Stellar Parameter and Chemical Abundances Pipeline (ASPCAP; García Pérez et al. 2016), and (iv) the maximum visual extinction from estimates of Galactic dust extinction (Bayestar17; Green et al. 2018).

Two additional constraints for statistical analysis include the maximum radius permissible for a background eclipsing object and the maximum depth of the secondary transit. These values were adopted from Morton et al. (2016) for KOI-929.01. For KOI-929.02, the centroid offsets from the *Kepler* data validation pipeline were used to determine the maximum radius. KOI-929.02 has centroid offsets of $\sim 1''.5$ and the maximum radius was set to a factor of three larger, at $4''.5$. The maximum depth of the secondary was set to five times the uncertainty in the secondary depth from the *Kepler* data validation pipeline. The Robo-AO contrast curve shown in Figure 1 is an additional constraint applied to the `vespa` analysis.

The results of the statistical analyses for Kepler-730 are shown in Table 2. The light curve for KOI-929.01 was validated only using the PDCSAP flux, detrended with a Gaussian process, and has an FPP of $(1.7 \pm 1.4) \times 10^{-4}$. The shallow transit depth of KOI-929.02 (~ 84 ppm) warranted the use of different detrending mechanisms to determine its susceptibility to changes in detrending. For this candidate, we performed statistical validation on both the SAP and PDCSAP flux detrended with three methods described in Section 2.2. The values and respective errors for each analysis were calculated as the mean and standard deviation of a bootstrap of 10 iterations of `vespa`. Regardless of the flux source and the detrending method, the signal was consistent with a statistically validated planet when adopting the threshold of FPP $< 1\%$ used in Morton et al. (2016).

3.3. RV Non-detection

The derived RVs (Section 2.1) folded to the period of the hot Jupiter, KOI-929.01, are shown in the first panel of Figure 2. No physical solution exists when adopting a standard Keplerian orbit and maximizing the likelihood. To determine if our RVs supported the existence of any companion, we used `thejoker` (Price-Whelan et al. 2017) to perform a rejection sampling analysis on the APOGEE-2 data. We performed the same analysis on the entire RV data set and the subset derived from spectra with $S/N > 10$ to determine if the quality of the data would mask a potential planet RV signal. We ran

$> 4 \times 10^6$ (2^{22}) samples with `thejoker` and more than 60,000 survived for each data set. The surviving samples are shown in the second panel of Figure 2. The underlying samples do not favor any orbital solutions between 1.5 days and twice the baseline of the APOGEE-2 observations (~ 411 days). The smallest stellar companion, a star at the hydrogen mass burning limit ($M_2 = 0.075 M_\odot$, $i = 90^\circ$, and $e = 0$), would induce observable reflex motion of Kepler-730 with an amplitude of a few km s^{-1} . `vespa` does not use RVs in the statistical analysis. Instead, a non-detection in RVs can bolster the statistical validation by reducing or eliminating the contribution of HEB/EB scenarios. The non-detection was most significant for the hot Jupiter, KOI-929.01, where the probability that the transit signal is not due to EBs or HEBs was $< 10^{-6}$. These low false positive probabilities suggest that Kepler-730 is, statistically, a multiplanet system.

4. System Parameters

We used the EXOFASTv2 analysis package (Eastman 2017) to model the photometry. The priors included (i) 2MASS *JHK* magnitudes, (ii) *UBV* magnitudes (Everett et al. 2012), (iii) *Wide-field Infrared Survey Explorer* magnitudes (Wright et al. 2010), (iv) spectroscopic parameters from ASPCAP, (v) maximum visual extinction from estimates of Galactic dust extinction from Bayestar17, and (vi) the distance estimate from Bailer-Jones et al. (2018). The spectroscopic parameters are derived from a combined spectrum, are empirically calibrated, and have been determined to be reliable (see Holtzman et al. 2018). The composite spectrum has a $S/N \approx 53$ per pixel and provides the following: $T_e = 5595 \pm 135$ K, $\log g \sim 4.06$, and $[\text{Fe}/\text{H}] = 0.21 \pm 0.02$. The surface gravity was poorly constrained during the calibration step and is only an initializing value for our analysis. Each planet had its period and time of mid-transit fixed to the value derived in DR25. The bottom row of Figure 2 presents the result of the fit to the photometry and Table 3 provides a summary of the stellar priors together with the inferred system parameters and respective confidence intervals.

The modeling reveals that Kepler-730 is a subgiant star with a radius of $1.411_{-0.051}^{+0.049} R_\odot$. It hosts a hot Jupiter and an interior Earth-sized planet with radii of $1.100_{-0.050}^{+0.047} R_{\text{Jup}}$ and $0.140 \pm 0.012 R_{\text{Jup}}$ ($1.57 \pm 0.13 R_\oplus$), respectively. To ensure that the derived parameters were consistent, we applied the diagnostic explored in Seager & Mallén-Ornelas (2003) for a transiting system and proceeded to estimate the primary stellar density from the photometry to be $0.537_{-0.048}^{+0.063}$ and $0.531_{-0.046}^{+0.060} \text{ g cm}^{-3}$ for KOI-929.01 and KOI-929.02, respectively. These values are consistent with each other and are in agreement with the density derived from the stellar models listed in Table 3. For comparison, the density of KIC 9141752 derived from stellar models is $3.48 \pm 0.45 \text{ g cm}^{-3}$.

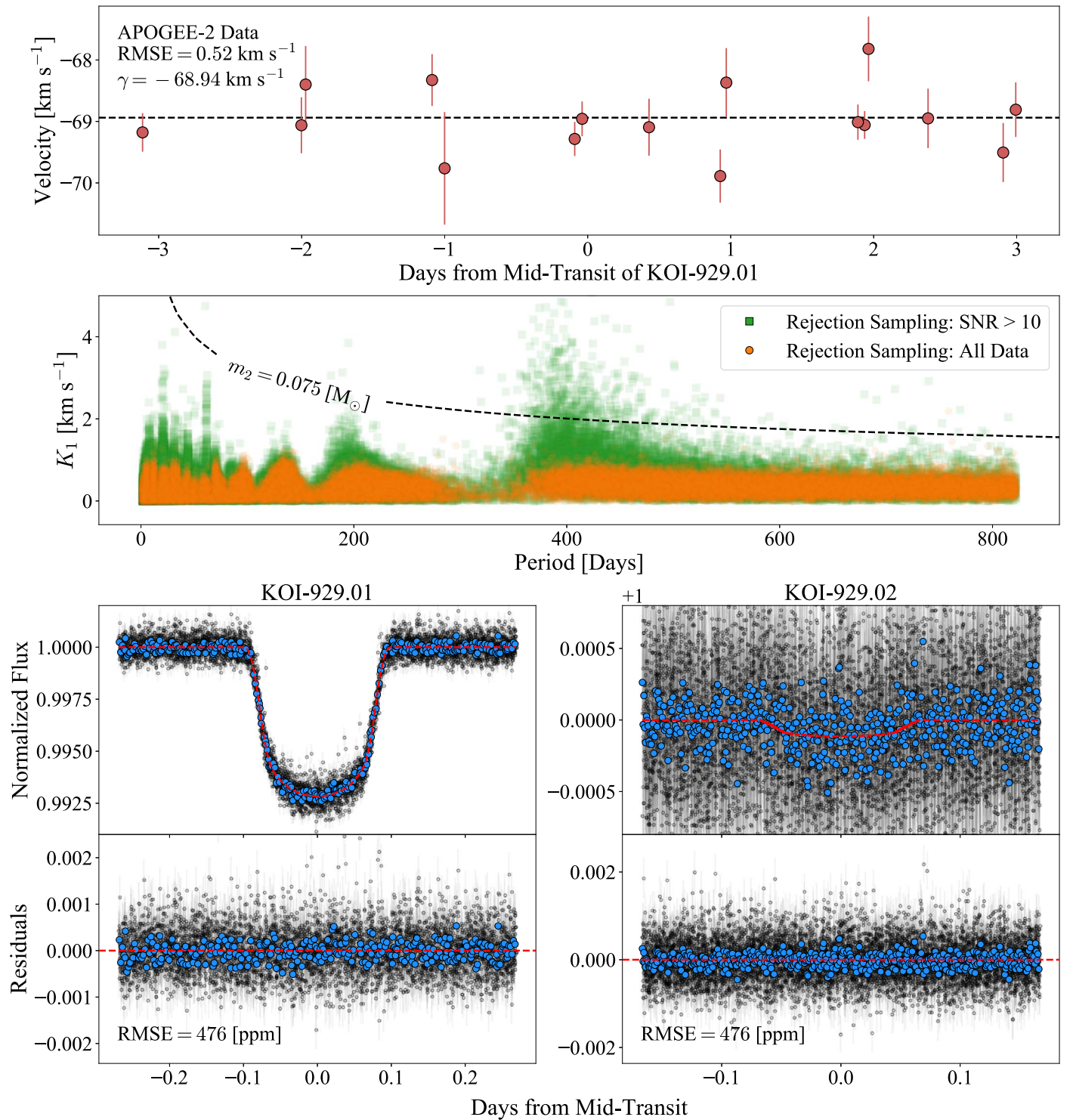


Figure 2. Velocimetry and photometry of Kepler-730. The top panel shows the radial velocities phased to the period of KOI-929.01. The middle panel presents the surviving population with $e < 0.5$ after rejection sampling. The contour for a star at the hydrogen mass burning limit (with $i = 90^\circ$ and $e = 0$) around Kepler-730 is plotted for reference. The code `thejoker` performed $> 4 \times 10^6$ (2^{22}) samplings and the large surviving population ($> 60,000$) demonstrates that our radial velocities are consistent with no statistically significant detection of a close stellar companion. The bottom row displays the phased light curves and best models with the rms error (RMSE). The small dots are the raw data and the larger circles are the data binned to a 1-minute cadence.

The impact parameters also set a lower limit for the mutual inclination at $\sim 3^\circ$. To investigate if a system hosting $1 M_\oplus$ and $1 M_{\text{Jup}}$ planets could exist in this configuration, we performed an N -body simulation with `whfast` (Rein & Tamayo 2015) spanning ~ 500 Myr. While we ignore forces other than gravity and any effects from stellar evolution, the fact that both planets

survived a long time suggests that a small mutual inclination does not necessitate chaotic evolution.

5. Discussion

The majority of currently detected hot Jupiters have no known close-in companions. The WASP-47 system was, until

Table 3
Parameters for the Kepler-730 System

Parameter	Units	Median Value	
Primary Stellar Priors:			
Effective Temperature ^a	T_e (K)	5595 ± 135	
Surface Gravity ^a	$\log(g_1)$ (cgs)	4.06	
Metallicity ^a	[Fe/H]	0.21 ± 0.02	
Maximum Visual Extinction	$A_{V,\max}$	0.126	
Distance	(pc)	1935 ± 122	
Primary Parameters:			
Mass	M_1 (M_\odot)	$1.047^{+0.072}_{-0.054}$	
Radius	R_1 (R_\odot)	$1.411^{+0.049}_{-0.051}$	
Density	ρ_1 (g cm^{-3})	$0.529^{+0.057}_{-0.046}$	
Surface Gravity	$\log(g_1)$ (cgs)	$4.162^{+0.032}_{-0.028}$	
Effective Temperature	T_e (K)	5620^{+55}_{-59}	
Metallicity	[Fe/H]	0.210 ± 0.014	
Age	(Gyr)	$9.5^{+2.5}_{-2.7}$	
Parallax	(mas)	$0.495^{+0.020}_{-0.019}$	
Linear Limb-darkening Coefficient	u_1	$0.418^{+0.028}_{-0.029}$	
Quadratic Limb-darkening Coefficient	u_2	0.235 ± 0.045	
Planetary Parameters:^b			
		b	c
Orbital Period	P (days)	6.491682808	2.851883380
Time of Mid-transit	T_C (BJD _{TDB})	2455007.633553	2454965.145500
Scaled Radius	R_p/R_1	$0.08013^{+0.00074}_{-0.00084}$	0.01025 ± 0.00074
Radius	R_p (R_{Jup})	$1.100^{+0.047}_{-0.050}$	0.140 ± 0.012
Scaled Semimajor Axis	a/R_1	$10.60^{+0.38}_{-0.32}$	$6.10^{+0.21}_{-0.18}$
Semimajor Axis	a (au)	$0.0694^{+0.0016}_{-0.0012}$	$0.03997^{+0.00089}_{-0.00069}$
Orbital Inclination	i (degrees)	$86.96^{+0.37}_{-0.31}$	$83.81^{+1.10}_{-0.83}$
Impact Parameter	b	$0.561^{+0.038}_{-0.050}$	$0.659^{+0.079}_{-0.110}$
Transit Duration	T_{14} (hr)	4.33 ± 0.03	2.76 ± 0.26
Equilibrium Temperature	T_{eq} (K)	1219^{+21}_{-22}	1607^{+27}_{-29}

Notes.

^a Values from ASPCAP.

^b P and T_C are fixed to the *Kepler* values. e and ω are null.

recently, the only known exception. In this Letter, we validated a second such system, Kepler-730, which hosts a hot Jupiter with an inner, transiting planet, and sheds new light on the origins of hot Jupiters. The analysis of *Gaia*, Robo-AO, *Kepler*, and APOGEE-2 data have revealed that the observed transits have a very high statistical probability of being genuine planets, and as such, provides independent validation of both Kepler-730b and Kepler-730c. The similar stellar densities derived from each transit further reinforces this conclusion. The *Kepler* transit timing observations catalog (Holczer et al. 2016) detected no timing variations, making it difficult to constrain the planetary masses. The non-detection of a Keplerian orbit in the APOGEE-2 velocimetry places an upper limit on the mass of the hot Jupiter of $\lesssim 13 M_{\text{Jup}}$, corresponding to a 3σ detection.

The existence of close-in companions in hot Jupiter systems is possible evidence that precludes a dynamically violent history. The measurement of stellar obliquity for the Kepler-730 system thus provides an unique chance to test if spin-orbit misalignment of hot Jupiters is a natural consequence of high-eccentricity migration. From the derived system parameters, we predict that the semi-amplitude of the Rossiter-McLaughlin effect for Kepler-730b is $\sim 12 \text{ m s}^{-1}$ (assuming $v \sin i \sim 2 \text{ km s}^{-1}$), which is marginally measurable with Keck/HIRES given the faintness of Kepler-730 (Wang et al. 2018a).

While tempting to discuss occurrence rates of such systems, we note that a significant fraction of the *Kepler* hot and warm

Jupiter sample has yet to be confirmed or statistically validated (Huang et al. 2016). Without additional observations, such as velocimetry, high-contrast imaging, and measured stellar parameters, a genuine false positive scenario can appear to be a statistically validated planet (e.g., Cañas et al. 2018). Our ongoing APOGEE-2 survey of KOIs will help investigate a significant fraction of this hot Jupiter sample, enabling a more accurate estimation of occurrence rates of WASP-47-like systems.











We thank Jon Jenkins, Christopher Spalding, and Wei Zhu for helpful discussion. S.W. thanks the Heising-Simons Foundation for their generous support. C.I.C. acknowledges support by NASA Headquarters under the NASA Earth and Space Science Fellowship Program—grant 80NSSC18K1114. C.I.C., C.F.B., and S.M. acknowledge support from NSF award AST 1517592. S.R.M. acknowledges support from NSF award AST 1616636. D.A.G.H. acknowledges support provided by the Spanish Ministry of Economy and Competitiveness (MINECO) under grant AYA-2017-88254-P.

Some of the data presented in this Letter were obtained from MAST. STScI is operated by the Association of Universities for Research in Astronomy, Inc., under NASA contract NAS5-26555. Support for MAST for non-*HST* data is provided by the NASA Office of Space Science via grant NNX09AF08G and by other grants and contracts. 2MASS is a joint project of the University of Massachusetts and IPAC at Caltech, funded by

NASA and the NSF. DSS was produced at STScI under USG grant NAG W-2166. Images of these surveys are based on photographic data obtained using the OST on Palomar Mountain and the UKST. The plates were processed into the present compressed digital form with the permission of these institutions. Funding for the *Kepler* mission is provided by the NASA Science Mission directorate. The NASA Exoplanet Archive is operated by Caltech, under contract with NASA under the Exoplanet Exploration Program.

Funding for SDSS-IV has been provided by the Alfred P. Sloan Foundation, the U.S. Department of Energy Office of Science, and the Participating Institutions. SDSS-IV acknowledges support and resources from the Center for High-Performance Computing at the University of Utah. The SDSS website is www.sdss.org. SDSS-IV is managed by the Astrophysical Research Consortium for the Participating Institutions of the SDSS Collaboration including the Brazilian Participation Group, the Carnegie Institution for Science, Carnegie Mellon University, the Chilean Participation Group, the French Participation Group, Harvard-Smithsonian Center for Astrophysics, Instituto de Astrofísica de Canarias, The Johns Hopkins University, Kavli Institute for the Physics and Mathematics of the Universe (IPMU)/University of Tokyo, Lawrence Berkeley National Laboratory, Leibniz Institut für Astrophysik Potsdam (AIP), Max-Planck-Institut für Astronomie (MPIA Heidelberg), Max-Planck-Institut für Astrophysik (MPA Garching), Max-Planck-Institut für Extraterrestrische Physik (MPE), National Astronomical Observatories of China, New Mexico State University, New York University, University of Notre Dame, Observatório Nacional/MCTI, The Ohio State University, Pennsylvania State University, Shanghai Astronomical Observatory, United Kingdom Participation Group, Universidad Nacional Autónoma de México, University of Arizona, University of Colorado Boulder, University of Oxford, University of Portsmouth, University of Utah, University of Virginia, University of Washington, University of Wisconsin, Vanderbilt University, and Yale University.

ORCID iDs

Caleb I. Cañas  <https://orcid.org/0000-0003-4835-0619>
 Suvrath Mahadevan  <https://orcid.org/0000-0001-9596-7983>
 Chad F. Bender  <https://orcid.org/0000-0003-4384-7220>
 Nathan De Lee  <https://orcid.org/0000-0002-3657-0705>
 Scott W. Fleming  <https://orcid.org/0000-0003-0556-027X>
 D. A. García-Hernández  <https://orcid.org/0000-0002-1693-2721>
 Fred R. Hearty  <https://orcid.org/0000-0002-1664-3102>
 Steven R. Majewski  <https://orcid.org/0000-0003-2025-3147>
 Alexandre Roman-Lopes  <https://orcid.org/0000-0002-1379-4204>
 Keivan G. Stassun  <https://orcid.org/0000-0002-3481-9052>

References

- Allard, F., Homeier, D., & Freytag, B. 2012, *RSPTA*, 370, 2765
 Bailer-Jones, C. A. L., Rybizki, J., Fouesneau, M., Mantelet, G., & Andrae, R. 2018, *AJ*, 156, 58
 Batygin, K., Bodenheimer, P. H., & Laughlin, G. P. 2016, *ApJ*, 829, 114
 Becker, J. C., Vanderburg, A., Adams, F. C., Rappaport, S. A., & Schwengel, H. M. 2015, *ApJL*, 812, L18
 Blanton, M. R., Bershad, M. A., Abolfathi, B., et al. 2017, *AJ*, 154, 28
 Borucki, W. J., Koch, D., Basri, G., et al. 2010, *Sci*, 327, 977
 Cañas, C. I., Bender, C. F., Mahadevan, S., et al. 2018, *ApJL*, 861, L4
 Dawson, R. I., & Johnson, J. A. 2018, *ARA&A*, 56, 175
 Eastman, J. 2017, EXOFASTv2: Generalized Publication-quality Exoplanet Modeling Code, Astrophysics Source Code Library, ascl:1710.003
 Everett, M. E., Howell, S. B., & Kinemuchi, K. 2012, *PASP*, 124, 316
 Fischer, D. A., Anglada-Escude, G., Arriagada, P., et al. 2016, *PASP*, 128, 066001
 Fleming, S. W., Mahadevan, S., Deshpande, R., et al. 2015, *AJ*, 149, 143
 Foreman-Mackey, D., Agol, E., Ambikasaran, S., & Angus, R. 2017, *AJ*, 154, 220
 Gaia Collaboration, Brown, A. G. A., Vallenari, A., et al. 2018, *A&A*, 616, A1
 García Pérez, A. E., Allende Prieto, C., Holtzman, J. A., et al. 2016, *AJ*, 151, 144
 Green, G. M., Schlafly, E. F., Finkbeiner, D., et al. 2018, *MNRAS*, 478, 651
 Gunn, J. E., Siegmund, W. A., Mannery, E. J., et al. 2006, *AJ*, 131, 2332
 Hellier, C., Anderson, D. R., Collier Cameron, A., et al. 2012, *MNRAS*, 426, 739
 Holczer, T., Mazeh, T., Nachmani, G., et al. 2016, *ApJS*, 225, 9
 Holtzman, J. A., Hasselquist, S., Shetrone, M., et al. 2018, *AJ*, 156, 125
 Huang, C., Wu, Y., & Triaud, A. H. M. J. 2016, *ApJ*, 825, 98
 Kipping, D. M., Hartman, J., Buchhave, L. A., et al. 2013, *ApJ*, 770, 101
 Lin, D. N. C., Bodenheimer, P., & Richardson, D. C. 1996, *Natur*, 380, 606
 Lissauer, J. J., Marcy, G. W., Bryson, S. T., et al. 2014, *ApJ*, 784, 44
 Majewski, S. R., Schiavon, R. P., Frinchaboy, P. M., et al. 2017, *AJ*, 154, 94
 Millholland, S., Wang, S., & Laughlin, G. 2017, *ApJL*, 849, L33
 Morton, T. D. 2015, Isochrones: Stellar Model Grid Package, Astrophysics Source Code Library, ascl:1503.010
 Morton, T. D., Bryson, S. T., Coughlin, J. L., et al. 2016, *ApJ*, 822, 86
 Nidever, D. L., Holtzman, J. A., Allende Prieto, C., et al. 2015, *AJ*, 150, 173
 Pepper, J., Stassun, K., & Gaudi, B. S. 2018, arXiv:1802.10158
 Petrovich, C. 2015, *ApJ*, 805, 75
 Price-Whelan, A. M., Hogg, D. W., Foreman-Mackey, D., & Rix, H.-W. 2017, *ApJ*, 837, 20
 Rasio, F. A., & Ford, E. B. 1996, *Sci*, 274, 954
 Rein, H., & Tamayo, D. 2015, *MNRAS*, 452, 376
 Seager, S., & Mallén-Ornelas, G. 2003, *ApJ*, 585, 1038
 Skrutskie, M. F., Cutri, R. M., Stiening, R., et al. 2006, *AJ*, 131, 1163
 Steffen, J. H., Ragozzine, D., Fabrycky, D. C., et al. 2012, *PNAS*, 109, 7982
 Stumpe, M. C., Smith, J. C., Van Cleve, J. E., et al. 2012, *PASP*, 124, 985
 Thompson, S. E., Coughlin, J. L., Hoffman, K., et al. 2018, *ApJS*, 235, 38
 Wang, S., Addison, B., Fischer, D. A., et al. 2018a, *AJ*, 155, 70
 Wang, S., Wang, X.-Y., Wang, Y.-H., et al. 2018b, *AJ*, 156, 181
 Wilson, J. C., Hearty, F., Skrutskie, M. F., et al. 2012, *Proc. SPIE*, 8446, 84460H
 Wright, E. L., Eisenhardt, P. R. M., Mainzer, A. K., et al. 2010, *AJ*, 140, 1868
 Wu, Y., & Lithwick, Y. 2011, *ApJ*, 735, 109
 Wu, Y., & Murray, N. 2003, *ApJ*, 589, 605
 Zasowski, G., Cohen, R. E., Chojnowski, S. D., et al. 2017, *AJ*, 154, 198
 Zhu, W., Dai, F., & Masuda, K. 2018, *RNAAS*, 2, 160
 Ziegler, C., Law, N. M., Baranec, C., et al. 2018, *AJ*, 156, 259
 Ziegler, C., Law, N. M., Morton, T., et al. 2017, *AJ*, 153, 66
 Zucker, S. 2003, *MNRAS*, 342, 1291